AGU PUBLICATIONS

JGR

Journal of Geophysical Research: Atmospheres

RESEARCH ARTICLE
10.1002/2016JD025795

Key Points:
- Moisture transport is modeled using 60 years of backward trajectories
- The decadal variation of precipitation can be attributed to variation of moisture source areas
- The Bay of Bengal and the South China Sea are major sources for rainfall in North China

Correspondence to:
Z. Jiang,
zhjiang@nuist.edu.cn

Citation:
Jiang, Z., S. Jiang, Y. Shi, Z. Liu, W. Li, and L. Li (2017), Impact of moisture source variation on decadal-scale changes of precipitation in North China from 1951 to 2010, *J. Geophys. Res. Atmos.*, *122*, 600–613, doi:10.1002/2016JD025795.

Received 25 AUG 2016
Accepted 16 NOV 2016
Accepted article online 18 NOV 2016
Published online 18 JAN 2017

The copyright line for this article was changed on 3 MAR 2017 after original online publication

Impact of moisture source variation on decadal-scale changes of precipitation in North China from 1951 to 2010

Zhihong Jiang[1], Shuai Jiang[1], Yi Shi[2], Zhengyu Liu[3], Wei Li[2], and Laurent Li[4]

[1]Key Laboratory of Meteorological Disaster of Ministry of Education, Collaborative Innovation Center on Forecast and Evaluation of Meteorological Disasters, Nanjing University of Information Science and Technology, Nanjing, China, [2]Joint International Research Laboratory of Climate and Environment Change, Collaborative Innovation Center on Forecast and Evaluation of Meteorological Disaster, Nanjing University of Information Science and Technology, Nanjing, China, [3]Center for Climatic Research, and Department of Atmospheric and Oceanic Sciences, University of Wisconsin-Madison, Madison, Wisconsin, USA, [4]Laboratoire de Météorologie Dynamique, CNRS, Sorbonne Universités, UPMC Univ Paris 06, Paris, France

Abstract The Hybrid Single-Particle Lagrangian Integrated Trajectory platform is employed in this study to simulate trajectories of air parcels in the rainy season in North China during last six decades (1951–2010), with the purpose of investigating moisture sources, their variation, and the eventual relationship with precipitation in North China. Climatological trajectories indicate that moisture in North China originates, respectively, from Eurasia (14.4%), eastern China (10.2%), the Bay of Bengal-South China Sea (33.8%), the Indian Ocean (10.7%), and the Pacific (30.9%). The spatiotemporal analysis of moisture trajectory based on extended empirical orthogonal function indicates that a decrease of precipitation in North China is caused mainly by a decrease of water vapor sources from the south, the Indian Ocean, the Bay of Bengal, and the South China Sea, which overwhelms an increase of water vapor sources from the North, mainly Eurasia, eastern China, and northern western North Pacific Ocean. In particular, the significant decrease of precipitation in the late 1970s (by 11.6%) is mainly caused by a 10.6% decrease of moisture from all sources. The Bay of Bengal, the South China Sea, and the Indian Ocean are dominant moisture source areas affecting the decadal-scale variation of precipitation in North China.

1. Introduction

Climate in North China manifests a strong monsoonal characteristic, with a significant portion of annual total rainfall in summer. The rainy season is generally in July and August when the monsoon front comes from the south and remains quasi-stationary in the region. Rainfall in North China experienced a significant variation during the last decades, with a severe reduction since the 1960s, especially around the 1970s, and an accompanying dry climate in North China [*Zhai et al*., 2005; *Ding et al*., 2008, 2009; *Zhu et al*., 2010].

Abundant water vapor supply is a necessary condition for summer precipitation in North China. Water vapor transport and balance, as well as their association with precipitation in North and East China, have been documented in a number of studies [*Zhai and Eskridge*, 1997; *Chen et al*., 1988; *Samel et al*., 1999; *Wei et al*., 2005]. They are generally very useful in understanding how the western Pacific subtropical high- and middle-latitude circulations play their main roles in modulating the water vapor transport and East Asian climate in summer at both interannual and interdecadal time scales. Accompanying the important weakening of the East Asian summer monsoon during the late 1970s [*Wang*, 2001, 2002], significant changes occurred in the related atmospheric circulation and precipitation pattern in eastern China [*Gong and Ho*, 2002; *Wang and Zhou*, 2005; *Han and Wang*, 2007]. Some authors pointed out that the increased summer rainfall in the Yangtze River valley in southeast China and the concurrent decrease of rainfall in North China after late 1970s were partly attributable to changes in the regional water vapor transport [*Wei et al*., 2005; *Ma and Gao*, 2006].

These studies, important in revealing the relationship between the rainfall and the regional water vapor balance, were however limited by their Eulerian approach that is unable to assess the moisture origins from remote source regions. Moisture fluxes across the regional boundaries cannot provide relevant information on the geographical sources of moisture due to the fast transition of wind fields [*Sodemann et al*., 2008].

Advanced methods have recently been developed to determine the moisture origin or sink by backward or forward trajectories of air parcels residing over the target region with Lagrangian models. Several models

such as Hybrid Single-Particle Lagrangian Integrated Trajectory (HYSPLIT) [*Draxler and Hess*, 1998; *Draxler and Rolph*, 2011] or FLEXible PARTicle [*Stohl et al*., 2005b] allow the calculation of back trajectories. The Lagrangian methodology has been successfully applied in studies on sources of moisture in many regions of the world: the Mackenzie River basin, North America [*Brimelow and Reuter*, 2005], southern Sweden [*Gustafsson et al*., 2010], northeast Spain [*Izquierdo et al*., 2012], the Sahel [*Nieto et al*., 2006; *Salih et al*., 2015], the South American monsoon area [*Drumond et al*., 2008], the Iberian Peninsula [*Gimeno et al*., 2010], and the Mediterranean Basin [*Nieto et al*., 2010; *Drumond et al*., 2011; *Gomez-Hernandez et al*., 2013], even the whole continental [*Gimeno et al*., 2012]. *Jiang et al*. [2011, 2013] and *Yang et al*. [2014], based on HYSPLIT, carried out an analysis of water vapor sources and transport to explain abnormal precipitations in East China. *Li et al*. [2016] detected the origins of moisture over southeast China based on HYSPLIT. *Huang and Cui* [2015], with a calculation of Lagrangian trajectories, investigated the moisture sources for strong rainfall events in the Sichuan Basin, China during summers of 2009–2013. *Bracken et al*. [2015], with HYSPLIT, documented the moisture sources for extreme rainfalls in the western U.S.

Those studies using a Lagrangian approach mainly focus on mean climate state or individual extreme events, few of them on interdecadal variability of water vapor sources and eventual relations with precipitation. It is thus a useful attempt that we devote our study to moisture variation originating from source areas and its connection with the precipitation pattern in North China during the last decades. In fact, understanding the persistent dry climate conditions in North China after late 1970s is our main motivation to conduct the present study employing a Lagrangian analysis.

A main challenge in using Lagrangian trajectories to deal with air parcels carrying water vapor is that water vapor is not a neutral gas in the atmosphere and it can strongly vary when transported. To remediate, *Stohl and James* [2004, 2005a] developed a method which incorporates the time derivative of humidity along the trajectories. It is a useful tool to assess origins of water vapor that falls during extreme precipitation events [*Stohl et al*., 2008]. Inspired by this concept, *Sun and Wang* [2014, 2015] analyzed major atmospheric moisture sources affecting West China and East China for a relatively short period of 10 years (2000–2009). Although such a methodology is useful and precise for individual precipitation events or short period, it is somehow computationally inefficient for long-term climate variation, beyond decadal time scales. Alternatively, we propose in this study to use simply the specific humidity as a weighting factor in calculating the density of trajectories. We believe that the variation of parcels (carrying moisture) originating from sources has certain relations with precipitation.

The article is organized as follows: the data and analyzing methods used in the study are described in section 2. Section 3 presents the variation of precipitation in North China, and section 4 contains a simple analysis of local moisture budget within the Eulerian framework in comparison to the Lagrangian method. Section 5, the main content of this article, contains the Lagrangian analysis results, together with some discussions. Conclusions are presented in section 6.

2. Data and Methods

2.1. Lagrangian Trajectory Calculation

The National Oceanic and Atmospheric Administration (NOAA) Hybrid Single-Particle Lagrangian Integrated Trajectory (HYSPLIT) model [*Draxler and Hess*, 1998] allows a user to simultaneously release parcels from all points within a user-specified matrix at a given time and height. These starting points do not necessarily have to be located on the data grid points, as HYSPLIT uses a bilinear interpolation to calculate meteorological variables at times and locations between the standard times and grid points available in the gridded data sets [*Brimelow and Reuter*, 2005]. The rainy season in North China is considered in this paper as from 19 July to 14 August, following *Liu and Ding* [2008]. The target area is defined as the box over North China (35°N–43°N, 110°E–120°E; the black rectangle box in Figure 1). The HYSPLIT model was run to calculate 264 h (11 days) backward air trajectories. The modeling period is from 00:00 UTC of 19 July to 00:00 UTC of 14 August for each year from 1951 to 2010 with an integration time step of 6 h. The target region is divided into $1° \times 1°$ grid points as starting parcels. Parcels are released at four levels including 500 m, 1500 m, 3000 m, and 5000 m or approximately 925 hPa, 850 hPa, 700 hPa, and 500 hPa. These levels are associated to main moisture transport paths for North China. All parcels were integrated backward in time, until 11 days. Outputs were recorded every 6 h with variables indicating the position (latitude, longitude, and altitude) and meteorological parameters (temperature, specific humidity, and geopotential height) [*Brimelow and Reuter*, 2005; *Gustafsson et al*., 2010].

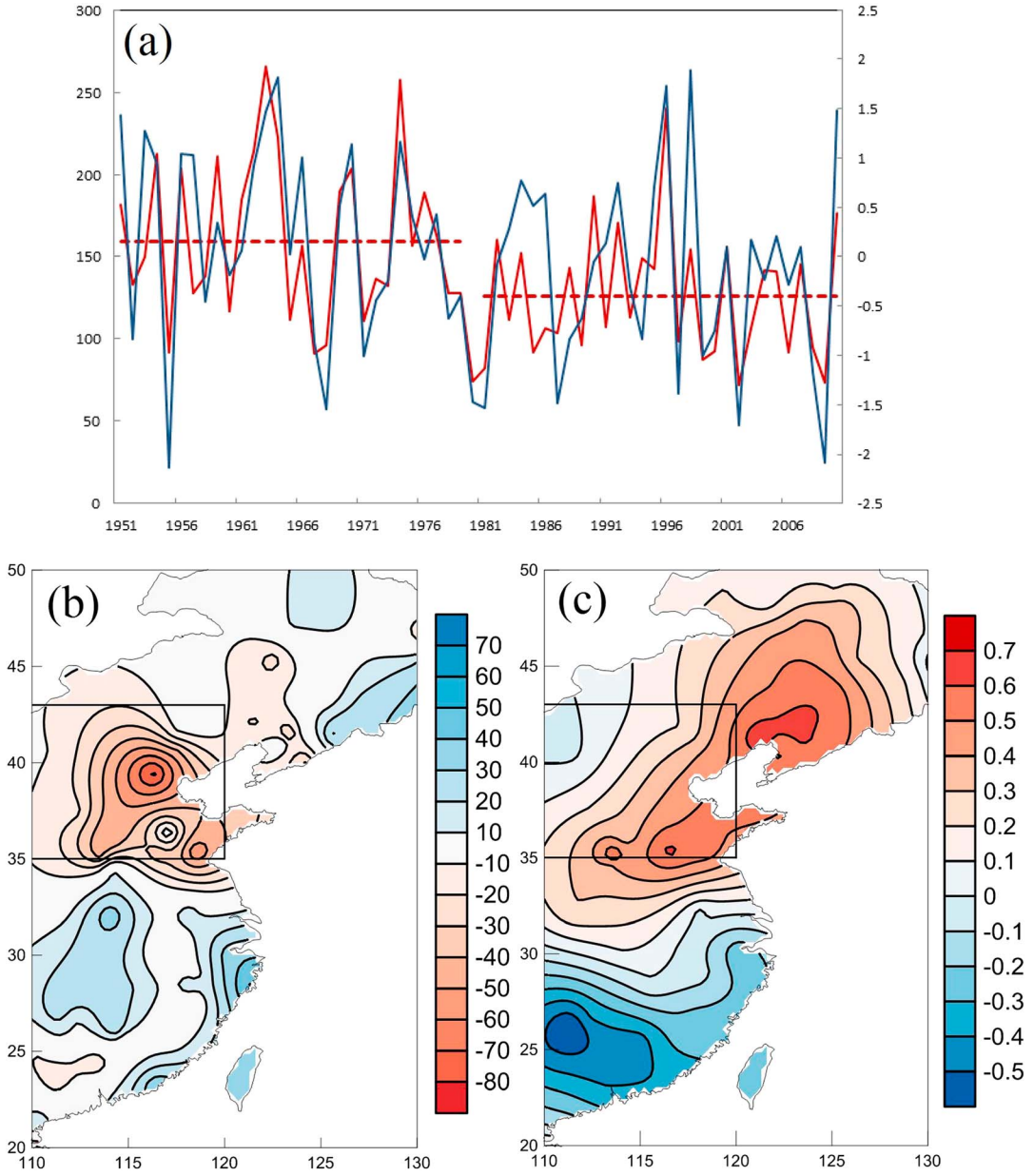

Figure 1. (a) The time series of regional average precipitation in North China during the rainy season (red line; left axis; unit: mm); the red dotted line is the average precipitation for the period of 1951–1980 and 1981–2010, superimposed with the leading principal component for the period of 1951–2010 (blue line; right axis with arbitrary unit). (b) The changes of summer precipitation (mm; from 19 July to 14 August) in East China (east of 110°E) from the period of 1951–1980 to 1981–2010; the black box denotes the study area in North China. (c) The leading EOF pattern of precipitation in East China (explained variance: 15.9%).

2.2. Data

Data used in this paper are from NOAA-National Centers for Environmental Prediction (NCEP)/National Center for Atmospheric Research (NCAR) reanalysis [*Kalnay et al.*, 1996]. Global pressure-level data were reprocessed into the HYSPLIT compatible format in the Air Resources Laboratory (ARL), NOAA, U.S. They are available from 1948 at 6 hourly temporal resolution and 2.5° (latitude/longitude grid) spatial resolution with 17 levels in the vertical. Data have been downloaded from the ARL's archives (http://ready.arl.noaa.gov/gbl_reanalysis.php). For daily rainfall, we use a data set provided and validated by the National Climate Center (NCC), China Meteorological Administration (http://ncc.cma.gov.cn), with 753 stations from 1951 to 2010 [*Lu et al.*, 2014].

After a quality control, we removed those stations whose observation sites were changed or record lengths are not sufficient, we finally keep 11 stations in North China.

3. Variability of Precipitation in North China

Previous studies indicated that precipitation in North China in the past decades had a strong interdecadal variability. There were two main regime shifts occurring in mid-1960s and 1980, respectively. The latter was believed to cause the long-lasting drought in the 1980s [*Zhou et al*., 2008; *Ding et al*., 2008, 2009]. In this study, we will first check these behaviors with the daily rainfall data set from NCC. The time series of regional accumulated precipitation in North China is calculated for the rainy season as from 19 July to 14 August and in our target area.

Figure 1a (red line) shows the time series of precipitation in North China; a notable interdecadal variation of precipitation can be found: a wet period from the 1950s to the mid-1970s, a dry period from the early 1980s to the early 1990s, and a relatively wet period appearing again from the mid-1990s onward. A notable wet-to-dry transition can be identified in the end of 1970s. Compared with 1951–1980, the regional average precipitation in North China decreases 11.6% in 1981–2010. So we plot the geographical changes of summer precipitation in East China from the period of 1951–1980 (first 30 years) to 1981–2010 (last 30 years) in Figure 1b. We can observe that precipitation significantly decreases in the north and increases in the south, presenting a dipole structure. Furthermore, we also performed an empirical orthogonal function (EOF) analysis on the precipitation in East China. Figure 1c displays the leading EOF pattern, with explained variance at 16%. There is also a visible dipole structure with the positive phase in the north and the negative phase in the south. The correlation coefficient between the series of leading principal component (Figure 1a, blue line) and the precipitation is 0.75, with a confidence level exceeding 99%. It is clear that the first EOF represents well the variation of precipitation in North China. We can also conclude that the rainfall variation in our target area is not a local phenomenon but coherent with rainfall variability at the regional scale of whole East China.

4. Moisture Flux and Budget Within the Eulerian Framework

We note that there is an abundant scientific literature investigating moisture budget in East and North China with an Eulerian approach. For the purpose of comparison with the Lagrangian method, moisture fluxes and budget within the Eulerian framework in North China are calculated with the NOAA-NCEP/NCAR reanalysis data. Just like the target region for Lagrangian backtracking trajectories, we select the same rectangular zone, representing North China (35°N–43°N, 110°E–120°E; Figure 1). Figure 2a shows the mean state (1951–2010) of the vertically integrated water vapor transport from ground to 300 hPa during the rainy season. The moisture mainly comes from the Eurasian continental westerlies and the monsoon wind from the south and southwest. So we assess the vertically integrated water vapor fluxes at the four boundaries separately (Figures 2b and 2c). The south and west boundaries show water vapor inflow into North China, with mean values of 102.9×10^6 kg s^{-1} from the south (60%) and 68.5×10^6 kg s^{-1} from the west (40%). The north and east boundaries show water vapor outflow. The net budget of water vapor transport (hereinafter referred to as local moisture budget; Figure 2b) shows a decreasing trend from 1951 to 2010. This decreasing moisture budget is caused by both decrease of water inflow at the south and west boundaries and increase of outflow at the east and north boundaries (Figure 2c).

Because of the notable interdecadal variation of precipitation, we calculate the changes of vertically integrated water vapor fluxes and divergences from the 30 years before 1980 to the 30 years after 1980. As shown in Figure 3, there is a significant transition in North China. Water vapor fluxes decrease at the south and west and increase at the east and north. The moisture divergence increases after 1980 in North China (Figure 3b), which indicates that the net water inflow decreases.

Although the Eulerian method can characterize the variation of moisture transport in a local area, it cannot describe climate characteristics at distant source areas. For example, Figure 2a shows the vertically integrated water vapor transport, but it is very hard to precisely determine the water vapor sources; the moisture in the west boundary may come from the Eurasian continental westerlies but also from the monsoon wind from the south and west. *Zhou et al*. [2008] argued that an imaginary line over the South China Sea (20°N, 110°E–120°E; Figures 2a and 2c), closer to the tropics, can be used as a proxy to characterize moisture sources for North China. But it is unprecise and cannot determine the moisture "whereabouts," as the moisture that goes

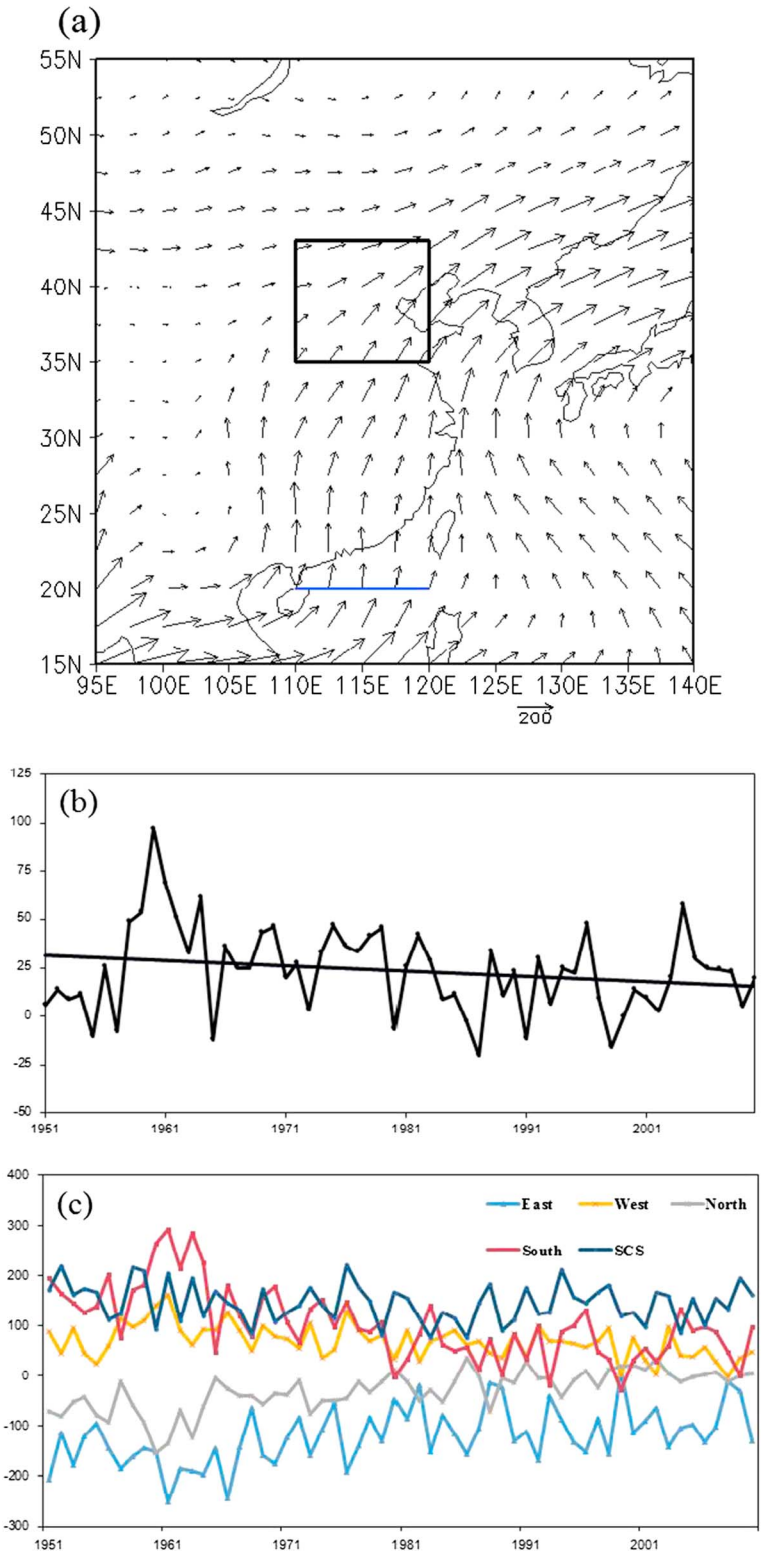

Figure 2. (a) The vertically integrated water vapor transport (vector; unit: kg/(m s)) from ground to 300 hPa in the rainy season (19 July to 14 August) from 1951 to 2010. The black box denotes the study area in North China, and the blue line denotes the water vapor path from the South China Sea (SCS). Water vapor flux through the area boundaries of North China. (b) The net water vapor transport flux of all boundaries (unit: 10^6 kg s^{-1}). (c) Water vapor transport fluxes through the four boundaries (east, west, south, and north) and an imaginary line in the South China Sea (SCS) as indicated in Figure 2a (unit: 10^6 kg s^{-1}).

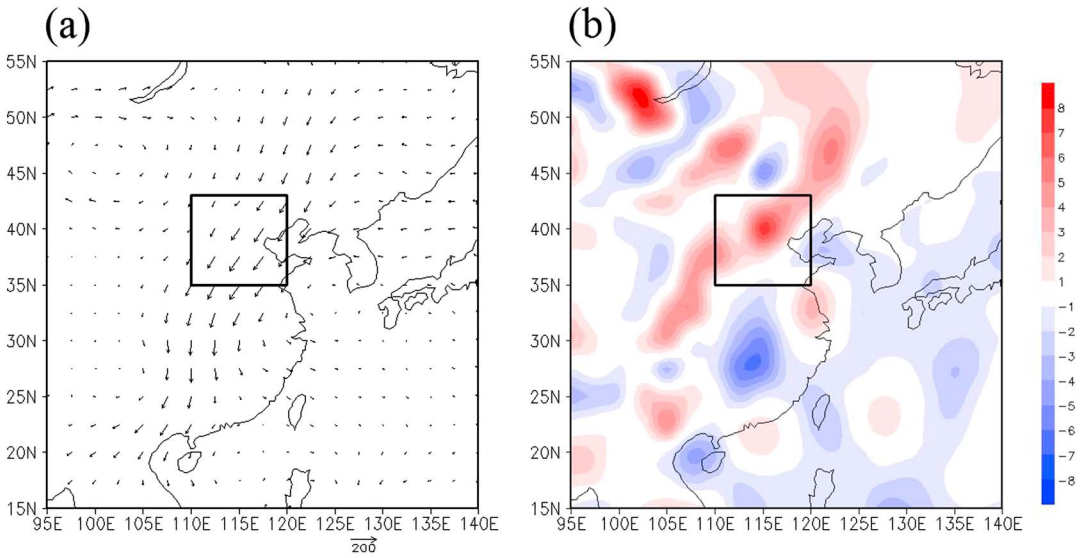

Figure 3. (a) Change of the vertically integrated water vapor transport (vector; unit: kg/(m s)) from 1951–1980 to 1981–2010. The black box denotes the study area in North China. (b) Changes of vertically integrated moisture divergence (shading; unit: 10^{-5} kg/(m^2 s)) from 1951–1980 to 1981–2010.

through the South China Sea boundary does not all reach North China. A Lagrangian analysis is thus necessary to determine moisture sources affecting rainfalls in North China.

5. Results and Discussions Based on the Lagrangian Analysis

5.1. Mean State of Moisture Sources

Back trajectories of air parcels were calculated until 11 days prior to their arriving into the domain. Outputs (including positions and relevant meteorological parameters) are binned into boxes of 2° × 2° in latitude-longitude for further diagnostics. The spatial evolution of air parcels location can approximately serve as the transport pathways. For a particular backward day, it is possible to account the total number of air parcels (or density of trajectories, if normalized by the size of boxes) reaching the target area, 4 times a day, and during the whole rainy season from 17 July to 14 August, each year. In our study, we focus on water vapor availability and transport, it is necessary to introduce the concept of moisture-weighted air parcels, the local specific humidity being a weighting factor. As the moisture in the atmosphere is mainly under 500 hPa, air parcels in the target area are having their starting elevation at four levels (925 hPa, 850 hPa, 700 hPa, and 500 hPa). These levels are associated to main moisture transport paths for North China.

Moisture source regions at climatological state are displayed in Figure 4, which shows, on a 2° × 2° grid, the total number of air parcels (4 times per day, during the season from 19 July to 14 August, each year), weighted by specific humidity (units: g/kg) for day 1 (Figure 4a), day 6 (Figure 4b), and day 11 (Figure 4c) prior to reaching North China. Results are averaged for the whole period. The mean height of air parcels is also calculated and shown in Figure 4 (shading). We can see that on day 1 prior to arriving (Figure 4a), air parcels mainly reside in North China and its surrounding areas, with an elongated form from southeast to northwest. Shading indicates the parcels' height located between 400 and 900 hPa, with a NW (high altitude)-SE (low altitude) orientation. It can be clearly observed (Figures 4b and 4c) that three dominating moisture transport pathways exist, in association to midlatitude circulations, the western Pacific subtropical high, and the Indian summer monsoon, respectively. This structure is consistent with our expectation, since summer monsoon precipitation in North China is generally related to the monsoonal front between cold air masses from the north and warm air masses from the south. On day 6 and day 11 (Figures 4b and 4c), the altitude of parcels from oceans is significantly lower than that from lands. Parcels are relatively rare from western Europe, the North Atlantic, and the Tibetan Plateau. Their altitude is generally between 400 hPa and 650 hPa. On day 11(Figure 4c), parcels pushed outward along three dominating pathways, which could be traced to the North Atlantic, western Europe, and a vast area from the western Indian Ocean to the

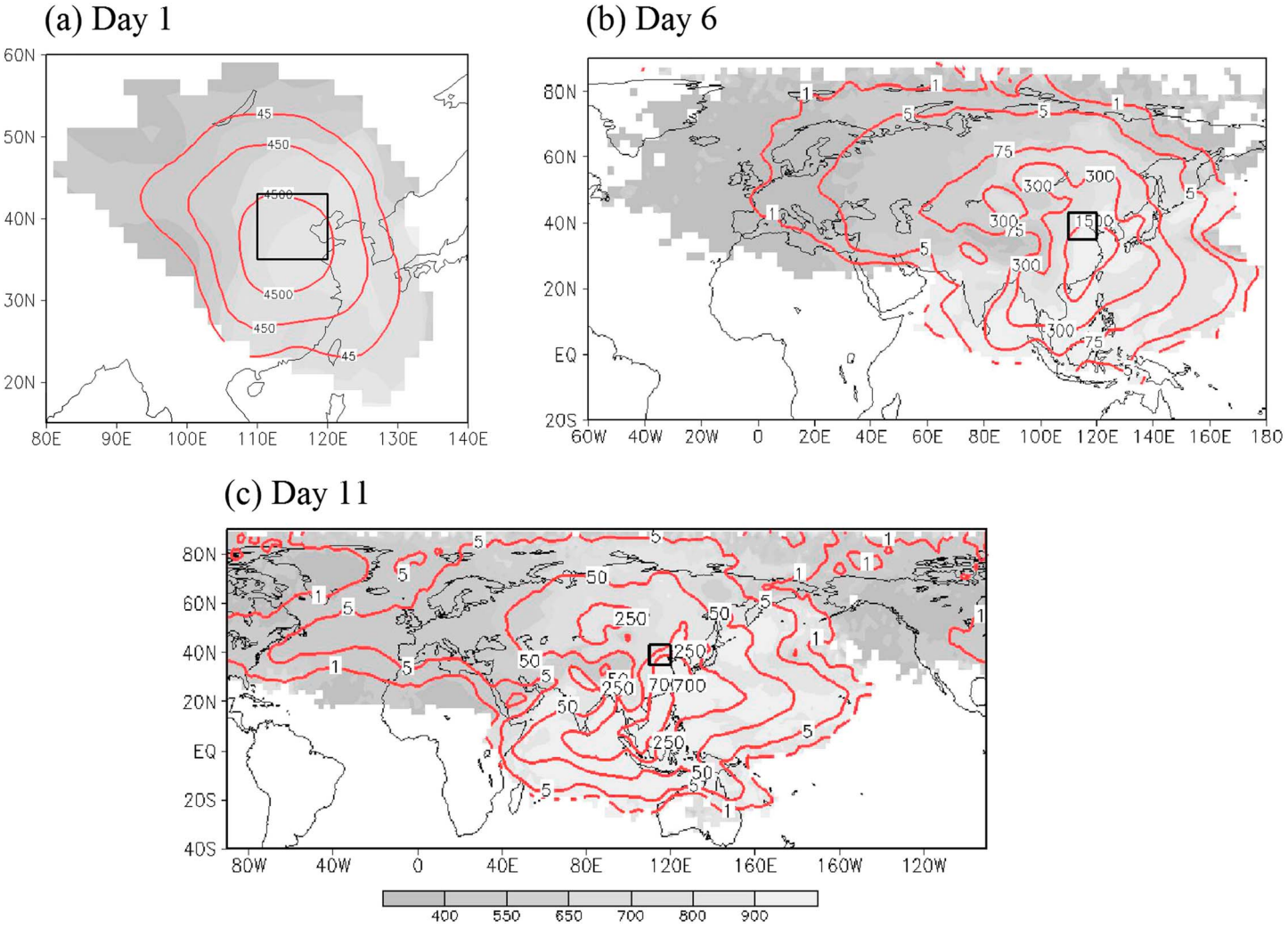

Figure 4. Number of particles weighted by specific humidity (units: g/kg) arriving in the domain of North China (the black rectangular zone) for (a) day 1, (b) day 6, and (c) day 11, respectively, prior to their arriving. The total number shown here corresponds to long-term annual means (1951 to 2010), calculated 4 times a day in the rainy season between 19 July and 14 August. The calculation was performed with the relevant water vapor (in g/kg) as a factor of multiplication. Geopotential heights (shading; unit: hPa) of parcels are also plotted.

middle Pacific. Main moisture sources on day 11 can be summarized as (1) Eurasia (EA), (2) eastern China (EC), (3) the Bay of Bengal and South China Sea (BSC), (4) the Indian Ocean (IO), and (5) the Pacific Ocean (PO).

5.2. Temporal and Spatial Variations of Moisture Sources

The dynamic transition of trajectories for air masses (carrying moisture) to reach North China from day 11 can be assessed with an extended EOF analysis of the consecutive trajectory patterns. We will focus on the leading mode (explained variance: 29.2%), which is highly correlated with the decadal shift in the 1970s.

Figure 5 shows the spatial pattern of the leading mode, displaying day 1 (Figure 5a), day 6 (Figure 5b), and day 11 (Figure 5c) (arbitrary units), respectively. The spatial pattern generally shows a dipole structure, with opposite signs between the south and the north for all days. Such an opposition reveals the relative importance of water vapor sources from either the north or the south. As can be seen in Figure 5a, the spatial pattern of day 1 mainly appears as a "southwest to northeast" dipole. The positive area is located in the Yangtze-Huaihe River basins and in south China, whereas the negative area is located in regions from

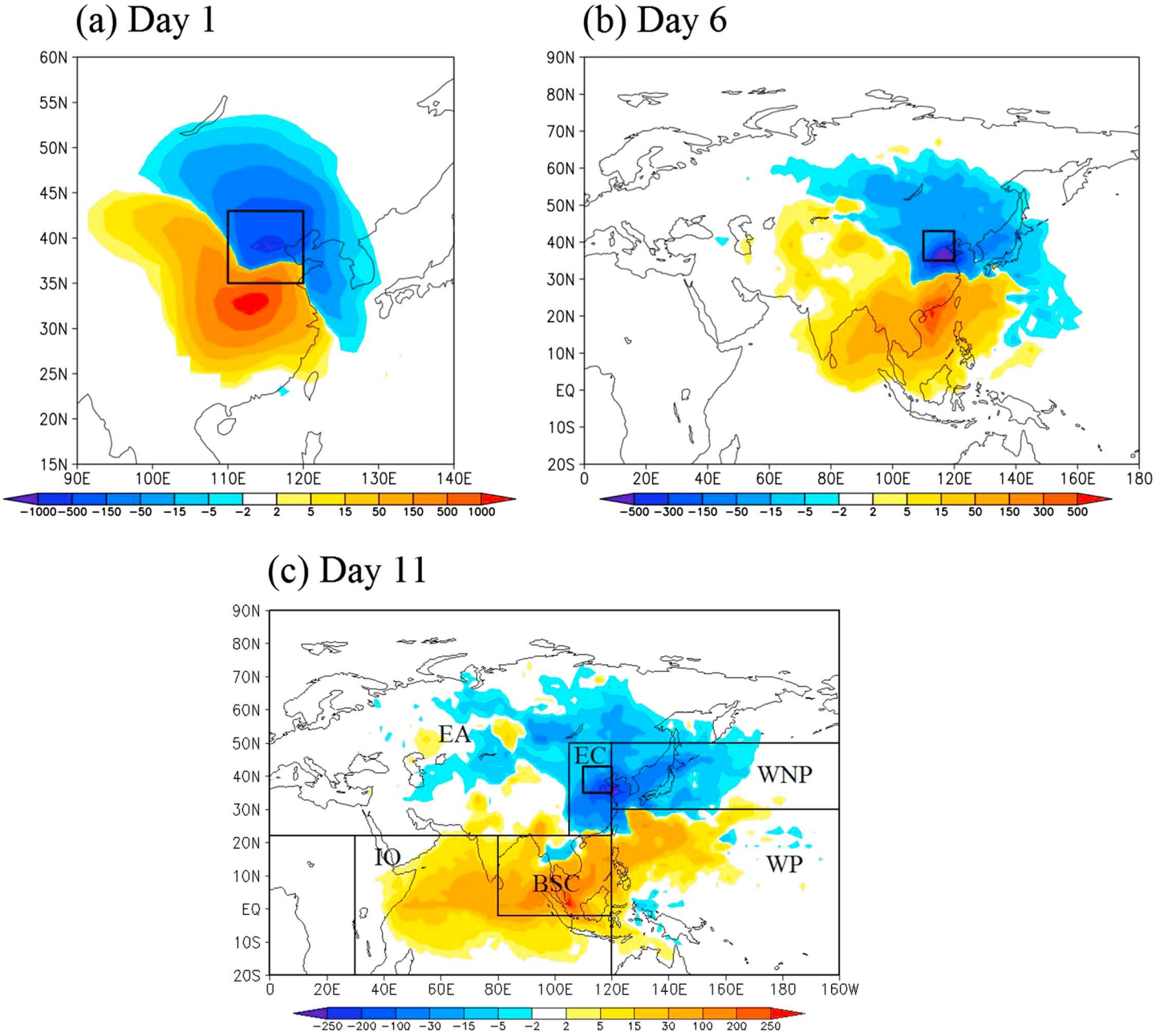

Figure 5. Leading mode of an extended EOF analysis performed on the total number of moisture-weighted parcels reaching the target region in North China. The transition of trajectories for days 1 to 11 prior to their arriving can be revealed through such an analysis. Days (a) 1, (b) 6, and (c) 11 are shown, respectively. The boxes in Figure 5c are the divisions for further investigations of water vapor sources affecting North China in summer.

North China to Baikal Lake. Figure 5b shows that the day 6 spatial pattern becomes a "south to north" dipole pattern, with positive and negative centers both pushing outward. The positive centers included parts of the India Ocean, the Bay of Bengal, the South China Sea, and the northwestern Pacific Ocean. Negative regions comprise an area from North China to central Siberia, the Sea of Japan, and the area east to it. Figure 5c shows that the 11th day spatial pattern is also a "south to north" dipole with a further extension for both positive and negative areas. The positive area is located over the India Ocean, the Bay of Bengal-South China Sea area, and south of 30°N in the Pacific Ocean. The negative area is located over a vast region of Eurasia, eastern China, and north of 30°N in the Pacific Ocean.

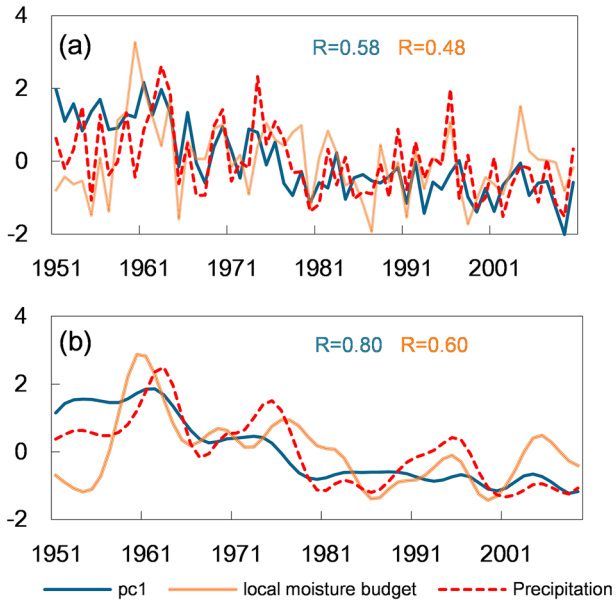

Figure 6. (a) Leading principal component of moisture source areas from the Lagrangian back trajectory calculation (blue curve), superimposed with local moisture budget obtained from the Eulerian calculation (purple curve; the same as in Figure 2b), and regional precipitation in North China (red dotted curve). All curves are normalized by their own standard deviation to facilitate their visual inspection. (b) The same as in Figure 6a but with a low-pass filter (with time scales >9 years) to show the interdecadal variation. *R*, marked with color (blue or purple), denotes the correlation coefficients between the moisture time series (leading PC or local moisture budget) and the precipitation.

Figure 6 shows the time coefficient (PC1) of the leading mode (blue curve in both plots). It shows a clear negative transition in the late 1970s. The dipole response discussed above can therefore be interpreted as follows. Prior to the transition, water vapor sources from the south are more abundant than those from the north. The reverse situation is observed after the transition. As an example for the day 11, more water vapor sources originate from Eurasia, eastern China, and north of 30°N in the Pacific Ocean after 1980, while water vapor sources from the Indian Ocean, the Bay of Bengal, the South China Sea, and south of 30°N in the Pacific Ocean decrease. *Ma and Gao* [2006] also pointed out that, in the 1950s and 1960s, water vapor in North China mainly comes from the south and southwest, and after the 1980s, water vapor from the northwest increases.

To confirm the robustness of results obtained with an extended EOF analysis for the 11 day sequences, we also performed individual-day EOF analyses. They generally show consistent results for both the spatial structure and temporal evolution. Correlation coefficients between the corresponding time series vary between 0.87 and 0.99. Since Figure 6 shows a clear separation of two regimes before and after 1980, we can furthermore verify our results by making the difference between the two periods. Results also largely confirm our conclusion from the extended EOF analysis.

It is worth mentioning that there is consistency between the Eularian and Lagrangian approaches. Figure 5a shows the spatial pattern on day 1, which generally displays a dipole structure, with opposite signs between the south and the north. The north and east (south) boundaries are basically located in negative (positive) areas indicating an increasing (a decreasing) tendency. This is consistent with the variation of water vapor fluxes at the three boundaries in North China in section 3 (Figure 2c).

5.3. Relationship Between Precipitation in North China and Moisture Transport

Let us now compare the results of regional moisture budget and sources of moisture transport with the regional precipitation in North China during the rainy season. Figure 6a displays the leading principal component from the extended EOF analysis applied to back trajectories, the local moisture budget, and the regional precipitation in North China. To facilitate the intercomparison, the three time series are all normalized by their own standard deviation. Our results provide a plausible explanation for the rainfall variation in North China during the last decades. It is clear that both the leading PC and the local moisture budget have a good correlation with the regional precipitation. Their correlation coefficient reaches 0.58 and 0.48, respectively. They are statistically significant at the 99.9% confidence level. Figure 6b presents the same time series but after filtering out variations shorter than 9 years. Both PC1 and local moisture budget show a reduction in the mid-1960s and the mid-1970s. There is a significant decreasing trend in the studied period, consistent with the regional precipitation trend. The two correlation coefficients become 0.80 and 0.60, statistically significant at the 99.9% confidence level. Both Eulerian and Lagrangian approaches provide very useful diagnostics for regional precipitation variation in North China, especially at interdecadal time scale.

Table 1. Precipitation, Climatological Mean (1951–2010; Unit: %) of Each Source, and the Sum Contribution for Moisture-Weighted Parcels (Number of Parcels)[a]

Source	EA	EC	WNP	IO	WP	BSC	SUM	Precipitation
Mean	19.5 (46.0)	8.6 (5.7)	9.0 (7.5)	12.1 (8.5)	19.4 (13.7)	31.4 (18.6)	100 (100)	100
P1	7.9 (18.8)	3.3 (2.0)	3.5 (2.7)	8.7 (6.0)	11.8 (8.4)	20.1 (12.1)	55.3 (50.0)	55.8
P2	11.6 (27.2)	5.3 (3.7)	5.5 (4.8)	3.4 (2.5)	7.6 (5.3)	11.3 (6.5)	44.7 (50.0)	44.2
P2 − P1	3.7 (8.4)	2.0 (1.7)	2.0 (2.1)	−5.3 (−3.5)	−4.2 (−3.1)	−8.8 (−5.6)	−10.6 (0)	−11.6

[a]P1 and P2 stand for the values before and after 1980. P2 − P1 denotes the difference.

In summary, the precipitation variation in North China is closely related to a "seesaw" structure for moisture source areas, during the last 60 years at interdecadal time scale. An important transition took place around the late 1970s. Prior to the transition, water vapor sources from the south were more abundant than those from the north. This favors precipitation increase in North China. But after 1980, the water vapor from southern sources decreased, which corresponds to precipitation decrease in North China.

5.4. Assessment of Moisture Sources

To make a quantitative assessment for moisture sources affecting rainfall in North China, we use the distribution of air parcels at day 11 prior to their arriving in North China and define five key regions: (1) Eurasia (EA), (2) eastern China (EC), (3) the Bay of Bengal and South China Sea (BSC), (4) the Indian Ocean (IO), and (5) the Pacific Ocean (PO). Since there is an opposite change between the north and south of 30°N in the Pacific Ocean as shown in section 5.2, we further divided the Pacific Ocean into two parts: northwest Pacific (WNP) and western Pacific (WP) (Figure 5c). The contribution of each area is evaluated as the proportion of air parcels (at day 11 priori to their arriving), residing in the region compared to the total number of air parcels. We should note that the calculation can be applied not only for the number of air parcels but also for a weighted amount by considering the relevant specific humidity (in g/kg) into account. This ensures a best assessment of both number of simple parcels and moisture transport from long-distance source.

BSC is the most important moisture source for North China with a climatological mean contribution (Table 1) of 31.4% during 1951–2010, followed by EA (19.5%), WP (19.4%), IO (12.1%), WNP (9.0%), and EC (8.6%). The Pacific accounts for a total of 28.4%. In terms of simple parcels, the contribution from EA increases to 46.0%, but that from BSC decreases to 18.6%, other regions remaining at a similar level. It is clear that moisture-weighted parcels show a certain advantage over the simple number of parcels if our main interest is on the water vapor transport (it is so, indeed). However, we should point out that in terms of temporal variation (in particular, at decadal scale), the two measures show very close results. Figure 7 shows the temporal evolution of regional contributions from 1951 to 2010, blue curves for moisture-weighed parcels and purple curves for simple parcels. We can observe that air parcels originated from EA, EC, and WNP show a growing tendency, but those from IO and BSC show a clear decline. Before the mid-1960s, moisture hardly originated from EA. But there is an obvious rising tendency from the mid-1960s to 1980s. The moisture contribution from EC shows a persistent increase for nearly six decades, which is associated with increasing evaporation under the background of global warming. For WNP, before the mid-1960s, few water vapor parcels originated from it, but they increased significantly since the late 1960s. There was a decrease in mid-1980s. Contributions for simple parcels change similarly in both EC and WNP. Moisture from IO shows a significant downtrend. It was abundant before the mid-1970s and reached the upmost level in 1963, then decreased rapidly from the early 1960s to the 1980s, and remains steady from the 1980s to the 21st century. The situation over BSC is very similar to that over IO: water vapor transport diminished steeply and presented a significant interdecadal variation. The water vapor transport over IO and BSC is found to be decreasing rapidly from the mid-1960s to the 1980s, which is closely related to the decadal-scale reduction of precipitation over North China in the same period. A decline also occurs for water vapor sources from WP, but the downtrend was not marked. The change of contribution for number of parcels is similar to moisture-weighted parcels in IO, WP, and BSC.

To investigate further the decadal variation of precipitation in North China, we calculate the mean contributions of source areas before and after 1980 for moisture-weighed parcels and simple number of parcels.

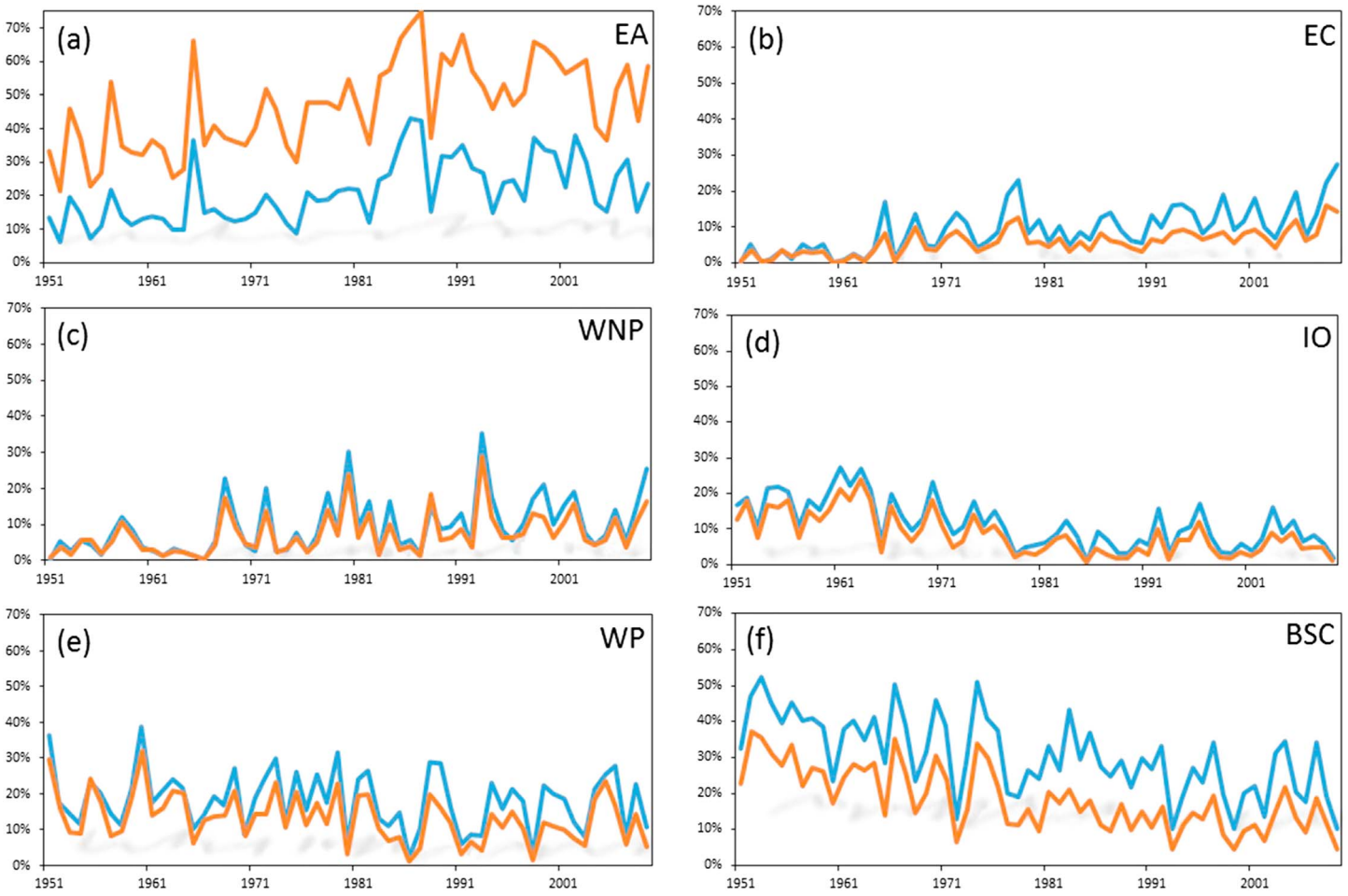

Figure 7. Evolution of moisture contribution (%) from (a) Eurasia (EA), (b) eastern China (EC), (c) northwest Pacific (WNP), (d) Indian Ocean (IO), (e) West Pacific (WP), and (f) the Bay of Bengal and South China Sea (BSC) during 1951–2010; the blue curves denote the moisture-weighed parcels and purple curves the simple parcels.

Differences between the two periods P1 (1951–1980) and P2 (1981–2010) are also shown in Table 1. The last column of the table (precipitation) indicates that all the precipitation during 1951–2010 fell in the period of climatological mean (1951–2010), P1 and P2.

BSC, WP, and IO are the three most important sources for North China in terms of moisture-weighted parcels (number of parcels) before 1980, which account for 40.6% (26.5%). But after 1980, they account for 22.3% (14.3%) only. Especially, contributions from BSC and IO decreased by 8.8% (5.6%) and 5.3% (3.5%), respectively (Table 1). On the contrary, contributions from EA, EC, and WNP increased. The contribution from EA increased significantly by 3.7% (8.4%), and the Pacific (WP and WNP) showed little changes. Transport of total moisture from the sources reduced by 10.6% after 1980 (1981–2010), compared to that before 1980 (1951–1980), which is an important factor contributing to the decrease of precipitation estimated at 11.6%. In terms of number of simple air parcels, of course, there is no change from year to year, since it remains constant by definition.

In summary, moisture sources for our target area in North China are fundamentally divided into north and south branches. For the last six decades, moisture contributions from EC, EA, and WNP showed a rising tendency, while that from IO and BSC had a downward trend (downward trend over WP is not significant). In terms of water vapor budget, increased water vapor contribution from the north (smaller specific humidity) is not able to offset the decreased water vapor contribution from the south, thereby decreasing the overall water vapor budget. IO and BSC are the key source areas with a significant decrease around 1980, affecting the decadal-scale reduction of precipitation in North China.

6. Conclusion and Discussion

In this paper, we used HYSPLIT, an objective Lagrangian model, to detect long-distance moisture sources affecting the precipitation in North China during last six decades (1951–2010). The applied method allowed not only the assessment of moisture sources for North China but also the quantification of moisture transport originating from these sources. North China experienced an important variability in summer precipitation during the last 60 years. The rainfall variability is revealed to be strongly correlated to changes in moisture source areas. Main findings are summarized as follows:

1. The moisture source regions for North China cover vast areas comprising Eurasia, the West Pacific, the Indian Ocean, and the South China Sea. We identified five important moisture source regions affecting North China: Eurasia (19.5%), eastern China (8.6%), the Bay of Bengal-South China Sea (31.4%), the Indian Ocean (12.1%), and the Pacific (28.4%). The Bay of Bengal, the South China Sea, and the Indian Ocean are the dominant moisture source areas affecting the precipitation in North China. The pathways for moisture to come from different sources are controlled by the dominant airflows associated with midlatitude circulations, the western Pacific subtropical high, and the Indian summer monsoon. Some of the moisture parcel trajectories present complicated transport structures from distant source areas.
2. The spatiotemporal analysis based on extended EOF indicates that the spatial distribution of parcels trajectories is primarily characterized by a south-north oriented dipole. The corresponding time coefficient shows a significant transition in the late 1970s. Prior to the transition, more water vapor sources originated from the Indian Ocean, the Bay of Bengal, the South China Sea, and south of 30°N in the Pacific Ocean, while fewer sources from Eurasia, eastern China, and north of 30°N in the Pacific Ocean. This favors more precipitation in North China. But after 1980, the water vapor from southern sources decreased, which corresponds to precipitation decrease in North China.
3. A quantitative assessment of moisture sources indicates that there is a reduction of 10.6% in 1981–2010, compared to 1951–1980, while precipitation in North China decreases by 11.6%. During the last six decades, air parcels with smaller moisture originated from Eurasia, eastern China, and the North Pacific Ocean showed a rising tendency, while those from the Indian Ocean, the South China Sea, and the tropical Pacific showed a decreasing trend. The concurrent increase of air parcels from the north (with less humidity) and decrease of air parcels from the south (with more humidity) are the main drivers for the reduction of rainfall in North China. The Bay of Bengal, the South China Sea, and the Indian Ocean are the dominant moisture source areas affecting the precipitation in North China.

Accompanying this interdecadal variability of the moisture sources in North China around the late 1970s, large-scale circulation features in the East Asian monsoon region also experienced important variations [*Hu*, 1997; *Goswami*, 2006; *Wang*, 2001, 2002; *Ding et al*., 2008, 2009]. In particular, we can note a change from anomalously strong summer monsoon flow to anomalously weak monsoon flow since the late 1970s [*Wang*, 2001] and a change from warming to cooling in the high troposphere in East Asia [*Xin et al*., 2008]. It is also striking that the anomalously strong low-pressure trough was replaced by an anomalously strong high pressure in middle and high latitudes in Asia [*Ding et al*., 2009]. Since the late 1970s, the weakening of the atmospheric heating over the Tibetan Plateau in combination with positive sea surface temperature anomalies and atmospheric heating in the tropical Pacific and Indian Oceans leads to a significant reduction of the land-sea thermal contrast and the tropospheric meridional and zonal temperature gradients over East Asia [*Chen and Wu*, 2000; *Qian et al*., 2003], which is partly responsible for the weakening of the Asian summer monsoon. These changes in large-scale circulation and thermodynamics lead to significant weakening of northward moisture transport from remote sources. It is clear that the variability of moisture transport over North China is not an isolated regional phenomenon but the consequence of significant changes in the Asian or East Asian climate system. *Song et al*. [2014] indicated that the heavy air pollution over China with a strong aerosol loading might cause a surface cooling, a weakened land-sea thermal contrast, and positive sea level pressure anomalies over North China, which is unfavorable for water vapor sources from the south.

It is worth mentioning that the analysis method reported here is suitable not only for North China but also for other domains. We are planning to investigate other areas of the rainfall dipole variability [*Ding et al*., 2008], mainly the increasing pole in South China. We also need to point out that all conclusions from the Lagrangian method are from a single realization with air parcels in the target area having their starting elevation at four particular levels (925, 850, 700, and 500 hPa). Although we could not precisely consider the whole-column

water vapor over North China, our calculation did provide relevant information on the origin of low-level atmospheric water vapor, which is the most relevant for rainfall. We also need to note that mixing between the air parcels and the surrounding air does occur when they are transported. Furthermore, moisture can be removed by precipitation or augmented by evapotranspiration from surface. These are important points for the Lagrangian approach of water vapor transport. Compared to methods already reported in literature, our methodology employing water vapor content as a weighting factor along the trajectories does provide a simple remediation for this issue.

Acknowledgments

We thank the Editor and anonymous reviewers for their constructive comments. We acknowledge the National Climate Center (NCC) of China (http://ncc.cma.gov.cn) for the observations and NOAA, the Air Resources Laboratory (ARL), from ARL's archives (http://ready.arl.noaa.gov/gbl_reanalysis.php) for NCEP/NCAR reanalysis data. This work is supported by the National Natural Science Foundation of China (41675081), the National Key Research and Development Program of China (grant 2016YFA0600402), and a project funded by the Priority Academic Program Development of Jiangsu Higher Education Institutions. Zhengyu Liu is partly supported by the U.S. NSF and DOE. Laurent Li is partly supported by the French ANR project China-Trend-Stream.

References

Bracken, C., B. Rajagopalan, M. Alexander, and S. Gangopadhyay (2015), Spatial variability of seasonal extreme precipitation in the western United States, *J. Geophys. Res. Atmos.*, *120*, 4522–4533, doi:10.1002/2015JD023205.

Brimelow, J. C., and G. W. Reuter (2005), Transport of atmospheric moisture during three extreme rainfall events over the Mackenzie River basin, *J. Hydrometeor*, *6*(4), 423–440.

Chen, L. T., and R. G. Wu (2000), Inter-annual and decadal variations of snowcover over Qinghai-Xizag Plateau and their relationship to summermonsoon rainfalls in China, *Adv. Atmos. Sci.*, *17*, 18–30.

Chen, T. C., M. C. Yen, and M. Murakami (1988), The water vapor transport associated with the 30–50 day oscillation over the Asian monsoon regions during 1979 summer, *Mon. Weather Rev.*, *116*, 1983–2002.

Ding, Y. H., Z. Y. Wang, and Y. Sun (2008), Inter-decadal variation of the summer precipitation in East China and its association with decreasing Asian summer monsoon. Part I. Observed evidences, *Int. J. Climatol.*, *28*, 1139–1161.

Ding, Y., Y. Sun, Z. Wang, Y. Zhu, and Y. Song (2009), Inter-decadal variation of the summer precipitation in China and its association with decreasing Asian summer monsoon. Part II : Possible cause, *Int. J. Climatol.*, *29*, 1926–1944.

Draxler, R. R., and G. Hess (1998), An overview of the HYSPLIT_4 modelling system for trajectories, *Aust. Meteorol. Mag.*, *47*(4), 295–308.

Draxler, R. R., and G. D. Rolph (2011), HYSPLIT (HYbrid Single-Particle Lagrangian Integrated Trajectory) Model; National Oceanic and Atmospheric Administration, *Air Resources Laboratory READY Web site*. ready. arl. noaa. gov/HYSPLIT. php, 2011.

Drumond, A., R. Nieto, L. Gimeno, and T. Ambrizzi (2008), A Lagrangian identification of major sources of moisture over central Brazil and La Plata Basin, *J. Geophys. Res.*, *113*, D14128, doi:10.1029/2007JD009547.

Drumond, A., R. Nieto, E. Hernandez, and L. Gimeno (2011), A Lagrangian analysis of the variation in moisture sources related to drier and wetter conditions in regions around the Mediterranean Basin, *Nat. Hazards Earth Syst. Sci.*, *11*, 2307–2320, doi:10.5194/nhess-11-2307-2011.

Gomez-Hernandez, M., A. Drumond, L. Gimeno, and R. Garcia-Herrera (2013), Variability of moisture sources in the Mediterranean region during the period 1980–2000, *Water Resour. Res.*, *49*, 6781–6794, doi:10.1002/wrcr.20538.

Gimeno, L., R. Nieto, R. M. Trigo, S. Vicente-Serrano, and J. I. López-Moreno (2010), Where does the Iberian Peninsula moisture come from? An answer based on a Lagrangian approach, *J. Hydrometeorol.*, *11*, 421–436, doi:10.1175/2009JHM1182.1.

Gimeno, L., A. Stohl, R. M. Trigo, F. Dominguez, K. Yoshimura, L. Yu, A. Drumond, A. M. Durán-Quesada, and R. Nieto (2012), Oceanic and terrestrial sources of continental precipitation, *Rev Geophys*, *50*, RG4003, doi:10.1029/2012RG000389.

Gong, D., and C. Ho (2002), Shift in the summer rainfall over the Yangtze River valley in the late 1970s, *Geophys. Res. Lett.*, *29*(10), 78–1, doi:10.1029/2001GL014523.

Goswami, B. N. (2006), The Asian monsoon: Interdecadal variability, in *The Asian Monsoon*, edited by B. Wang, pp. 295–328, Praxing Publishing, Chichester, U. K.

Gustafsson, M., D. Rayner, and D. Chen (2010), Extreme rainfall events in southern Sweden: Where does the moisture come from?, *Tellus, Ser. A*, *62*(5), 605–616.

Han, J., and H. Wang (2007), Interdecadal variability of the East Asian summer monsoon in an AGCM, *Adv. Atmos. Sci.*, *24*, 808–818, doi:10.1007/s00376-007-0808-0.

Hu, Z. Z. (1997), Interdecadal variability of summer climate over East Asia and its association with 500 hPa height and global sea surface temperature, *J. Geophys. Res.*, *102*(D16), 19,403–19,412, doi:10.1029/97JD01052.

Huang, Y., and X. Cui (2015), Moisture sources of torrential rainfall events in the Sichuan Basin of China during summers of 2009–2013, *J. Hydrometeorol.*, *16*, 1906–1917, doi:10.1175/jhm-d-14-0220.1.

Izquierdo, R., A. Avila, and M. Alarcón (2012), Trajectory statistical analysis of atmospheric transport patterns and trends in precipitation chemistry of a rural site in NE Spain in 1984–2009, *Atmos. Environ.*, *61*(12), 400–408.

Jiang, Z., Z. Liang, Z. Liu, and Y. Zhu (2011), A diagnostic study of water vapor transport and budget during heavy precipitation over the Huaihe River basin in 2007 [in Chinese], *Chin. J. Atmos. Sci.*, *35*, 361–372, doi:10.3878/j.issn.1006-9895.2011.02.14.

Jiang, Z., W. Ren, Z. Liu, and H. Yang (2013), Analysis of water vapor transport characteristics during the Meiyu over the Yangtze-Huaihe River valley using the Lagrangian method [in Chinese], *Acta Meteorol. Sin.*, *71*, 295–304, doi:10.11676/qxxb2013.017.

Kalnay, E., et al. (1996), The NCEP/NCAR 40-year reanalysis project, *Bull. Am. Meteorol. Soc.*, *77*, 437–471.

Li, X., W. Zhou, and Y. D. Chen (2016), Detecting the origins of moisture over southeast China: Seasonal variation and heavy rainfall, *Adv. Atmos. Sci.*, *33*(3), 319–329.

Liu, H., and Y. Ding (2008), The beginning and the end of flood season of North China and climatology analysis [in Chinese], *J. Appl. Meteorol. Sci.*, *19*, 688–696.

Lu, E., Y. Zeng, Y. Luo, Y. Ding, W. Zhao, S. Liu, L. Gong, Y. Jiang, Z. Jiang, and H. Chen (2014), Changes of summer precipitation in China: The dominanceof frequency and intensity and linkage with changes in moisture and air temperature, *J. Geophys. Res. Atmos.*, *119*, 12,575–12,587, doi:10.1002/2014JD022456.

Ma, J.-J., and X.-Q. Gao (2006), The transportation paths of water vapor and its relation to climate change over North China [in Chinese], *Plateau Meteorol.*, *25*, 893–899.

Nieto, R., L. Gimeno, and R. M. Trigo (2006), A Lagrangian identification of major sources of Sahel moisture, *Geophys. Res. Lett.*, *33*, L18707, doi:10.1029/2006GL027232.

Nieto, R., L. Gimeno, A. Drumond, and E. Hernandez (2010), A Lagrangian identification of the main moisture sources and sinks affecting the Mediterranean area, *WSEAS Trans. Environ. Dev.*, *5*(6), 365–374.

Qian, Y. F., Y. Q. Zheng, Y. Zhang, and M. Q. Miao (2003), Response of China's summer monsoon climate to snow anomaly over the Tibetan Plateau, *Int. J. Climatol.*, *23*, 593–613.

Salih, A. A. M., Q. Zhang, and M. Tjernström (2015), Lagrangian tracing of Sahelian Sudan moisture sources, *J. Geophys. Res. Atmos.*, *120*, 6793–6808, doi:10.1002/2015JD023238.

Samel, A. N., W. C. Wang, and X. Z. Liang (1999), The monsoon rainband over China and relationships with the Eurasian circulation, *J. Clim.*, *12*(12), 115–131, doi:10.1175/1520-0442-12.1.115.

Sodemann, H., C. Schwierz, and H. Wernli (2008), Interannual variability of Greenland winter precipitation sources: Lagrangian moisture diagnostic and North Atlantic Oscillation influence, *J. Geophys. Res.*, *113*, D03107, doi:10.1029/2007JD008503.

Stohl, A., and P. James (2004), A Lagrangian analysis of the atmospheric branch of the global water cycle. Part I: Method description, validation, and demonstration for the August 2002 flooding in central Europe, *J. Hydrometeorol.*, *5*(4), 656–678.

Stohl, A., and P. James (2005a), A Lagrangian analysis of the atmospheric branch of the global water cycle. Part II: Moisture transports between Earth's ocean basins and river catchments, *J. Hydrometeorol.*, *6*(6), doi:10.1175/JHM470.1.

Stohl, A., C. Forster, A. Frank, P. Seibert, and G. Wotawa (2005b), Technical note: The Lagrangian particle dispersion model FLEXPART version6.2, *Atmos. Chem. Phys.*, *5*, 2461–2474, doi:10.5194/acp-5-2461-2005.

Stohl, A., C. Forster, and H. Sodemann (2008), Remote sources of water vapor forming precipitation on the Norwegian west coast at 60°N—A tale of hurricanes and an atmospheric river, *J. Geophys. Res.*, *113*, D05102, doi:10.1029/2007JD009006.

Song, F. F., T. J. Zhou, and Y. Qian (2014), Responses of East Asian summer monsoon to natural and anthropogenic forcings in the 17 latest CMIP5 models, *Geophys. Res. Lett.*, *41*, 596–603, doi:10.1002/2013GL058705.

Sun, B., and H. Wang (2014), Moisture sources of semiarid grassland in China using the Lagrangian particle model FLEXPART, *J. Clim.*, *27*, 2457–2474, doi:10.1175/JCLI-D-13-00517.1.

Sun, B., and H. Wang (2015), Analysis of the major atmospheric moisture sources affecting three sub-regions of East China, *Int. J. Climatol.*, *35*, 2243–2257, doi:10.1002/joc.4145.

Wang, H. (2001), The weakening of the Asian monsoon circulation after the end of 1970s, *Adv. Atmos. Sci.*, *18*, 376–386, doi:10.1007/BF02919316.

Wang, H. (2002), The instability of the East Asian summer monsoon-ENSO relations, *Adv. Atmos. Sci.*, *19*, 1–11, doi:10.1007/s00376-002-0029-5.

Wang, Y., and L. Zhou (2005), Observed trends in extreme precipitation events in China during 1961–2001 and the associated changes in large-scale circulation, *Geophys. Res. Lett.*, *32*, L09707, doi:10.1029/2005GL022574.

Wei, J., Z. H. Lin, J. Xia, and S. Y. Tao (2005), Interannual and interdecadal variability of atmospheric water vapor transport in the Haihe River basin, *Pedosphere*, *15*, 585–594.

Xin, X., Z. Li, R. Yu, and T. Zhou (2008), Impacts of upper tropospheric cooling upon the late spring drought in East Asia simulated by a regional climate model, *Adv. Atmos. Sci.*, *25*(4), 555–562.

Yang, H., Z. Jiang, Z. Liu, and Q. Zhang (2014), Analysis of climatic characteristics of water vapor transport based on the Lagrangian method: A comparison between Meiyu in the Yangtze-Huaihe River region and the Huabei rainy season [in Chinese], *Chin. J. Atmos. Sci.*, *38*(5), 965–973, doi:10.3878/j.issn.1006-9895.1402.13228.

Zhai, P., and R. E. Eskridge (1997), Atmospheric water vapor over China, *J. Clim.*, *10*, 2643–2652, doi:10.1175/1520-0442(1997)010<2643:AWVOC>2.0.CO;2.

Zhai, P., X. Zhang, H. Wan, and X. Pan (2005), Trends in total precipitation and frequency of daily precipitation extremes over China, *J. Clim.*, *18*(7), 1096–1108.

Zhou, X., Y. Ding, and P. Wang (2008), Features of moisture transport associated with the precipitation over North China during July–August [in Chinese], *Chin. J. Atmos. Sci.*, *32*, 345–357, doi:10.3878/j.issn.1006-9895.2008.02.13.

Zhu, Y., H. Wang, W. Zhou, and J. Ma (2010), Recent changes in the summer precipitation pattern in East China and the background circulation, *Clim. Dyn.*, *36*, 1463–1473, doi:10.1007/s00382-010-0852-9.